THE SEARCH FOR WATER ICE AT THE LUNAR SOUTH POLE: A MINI-RF INVESTIGATION. L. M. Jozwiak[1], J. M. Leeburn[1], and G. W. Patterson[1], [1]Planetary Exploration Group, Johns Hopkins University Applied Physics Laboratory, Laurel, MD, USA. (Corresponding author: lauren.jozwiak@jhuapl.edu).

Introduction: Questions surrounding the presence, type, and extent of water ice at the lunar poles have driven a large number of studies by multiple instruments over the past two decade of lunar science. Sparked by observations of depressed neutrons in Lunar Prospector data [1, 2], and solidified by direct observations of water absorption in the LCROSS plume [3], multiple instruments onboard the LRO mission have sought to constrain the presence and distribution of water ice at the lunar poles. While several instruments have identified signatures consistent with surficial water frost [e.g. 4, 5], evidence for the persistence of these water ice deposits at depth has remained scant.

Due to the characteristic interaction between radar waves and water ice deposits [e.g. 6], several previous studies have attempted to identify the presence of water ice at the lunar south pole. Following the LCROSS impact, researchers studied both Mini-RF and Mini-SAR monostatic observations of the Cabeus impact location, however, they did not observe the characteristic coherent backscatter effect that would be expected if spatially significant ice deposits were present [7]. It was thus concluded that, if present, the ice deposits must be smaller than the sensing wavelength of the S-band radar (~12.6 cm).

Recent LOLA studies have suggested that broad-scale shallowing of simple craters at the lunar south pole is a result of buried ice lenses [8]. Furthermore, a study of LOLA-scale surface roughness in south polar craters has suggested increased smoothing in regions where water ice could be thermally stable in the near subsurface [9]. In this study, we use Mini-RF radar data to examine roughness variations in the near surface environment of 43 south polar craters representing a variety of thermal environments and illumination conditions to investigate whether unusual regions of exceptional smoothness exist, and if these regions are related to volatile processes.

Data Selection and Analysis: Our analysis leverages Mini-RF CPR data from a controlled polar mosaics produced by the USGS [10] in both the 0-180° (east-looking) and 180-360° (west-looking) geometries. These mosaics are fully georeferenced and co-registered to the LROC WAC 100 m global mosaic and the LOLA 512 ppd global topographic map. In addition to the CPR mosaics, we also utilized three Diviner-derived temperature maps: summer average, summer maximum, and winter minimum temperatures.

In order to define our floor analysis regions, we used a LOLA-derived slope map to isolate regions with slopes less than 5°. This slope threshold was selected so as to decrease the chance of increases in CPR as a result of interaction with sloped surfaces. Once we isolated low-slope regions, we used a LOLA-derived PSR catalog to separate the floor regions into PSR (permanently shadowed region), non PSR, and "mixed" for craters which contained both PSR and non-PSR crater floor regions (Fig. 1).

We selected a total of 43 craters: 11 PSR, 13 non PSR, and 19 mixed craters. Craters were selected to include sufficiently large floor regions for robust data counts (> 1000 CPR pixels), as well as, to include a range of geologic ages from the pre-Nectarian through Eratosthenian. In addition to craters, we also defined 7 background regions. The background regions were similarly restricted to slopes <5°, and with a variety of illumination conditions and geologic unit ages represented.

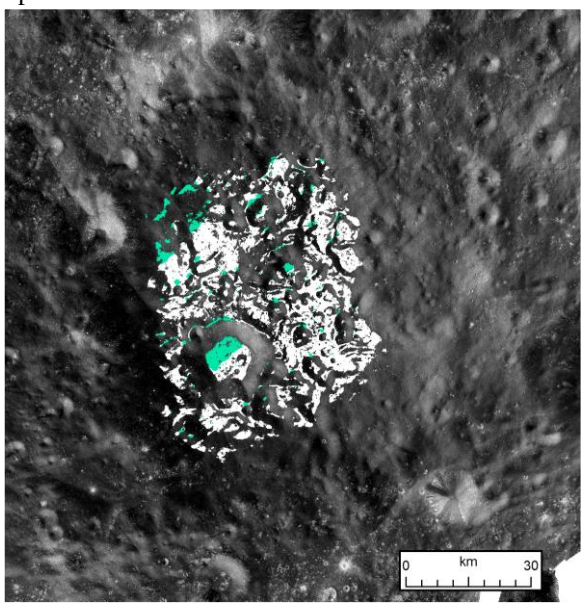

Figure 1: PSR (green) and non-PSR (white) shapefiles for the floor of Cabeus crater. Mini-RF monostatic east-looking mosaic basemap.

While the datasets were visualized, and shapefiles defined using the ArcGIS program, we utilized the Python shape.ly tool to extract statistics from each shapefile region, including minimum, maximum, median, mean, std. deviation, count number, and area. These parameters were extracted from both east- and

west-looking CPR mosaics, as well as, the Diviner temperature datasets. For each crater shapefile we plotted mean value ±1 std. deviation.

Results: The results of the east-looking CPR analysis are shown in Fig. 2. The craters are organized by floor illumination condition. A range of CPR values is immediately visible, as is the observation that illumination condition does not have a correlation with surface roughness (CPR). Figure 2, however, does highlight several unusually low CPR values, those falling below CPR values of 0.4. When correlated against the west-looking CPR data, we observe 5 craters with persistently low CPR: Cabeus, Cabeus B, Sverdrup, an unnamed crater located at 168.4°E, 88.7°S, and Laveran (R2, Fig. 2). During the initial Mini-RF monostatic analysis of Cabeus crater [7], it was noted that Cabeus displayed some of the lowest CPR values for the entire south polar region. This observation is borne out by our results, and extends this observation of exceptionally low CPR to several additional craters. The persistently low CPR craters identified by this study also have significant overlap with smooth craters identified by [9], including Cabeus, Cabeus B, and Sverdrup. Furthermore, the crater Laveran was identified by [8] as displaying an unusually shallow depth to diameter ratio, possibly indicative of subsurface ice.

Our analysis of Diviner temperature data suggests that while all of the craters with exceptionally low CPR have summer average temperatures below 112 K (the temperature required for stable surface ice [4]), this thermal requirement does not appear to drive low CPRs, and many craters meet this temperature threshold without displaying similarly low CPR.

Discussion: Our results have identified a set of 5 craters with anomalous, persistently low CPR at the south pole. When compared with other average lunar terrains [11], and the broad south polar averages, this difference becomes more pronounced (Fig. 3). Indeed the magnitude of difference between the exceptionally low CPR craters and the smoothest nearside terrains (nearside radar dark terrains), is the magnitude difference as between nearside dark (smooth) terrains and farside rough (bright) terrains. By this metric, these craters could thus be defined as a new class of exceptionally low CPR/exceptionally smooth craters.

The correlation of these craters with other LRO datasets indicative of water ice suggests that the exceptional smoothness could be the result of volatile-related processes. As CPR reflects a roughness in the upper volume of regolith, these exceptionally low CPR values suggest a fine-grained region largely devoid of any scatterers. This could be consistent with an intimate regolith+ice mixture with relatively low porosity, and individual ice grains well below the S-band sensing wavelength. We are working to extend this analysis to non-crater regions of the south pole, as well as, to more fully explore both volatile-related and non-volatile related causal mechanisms for these exceptionally low CPR values.

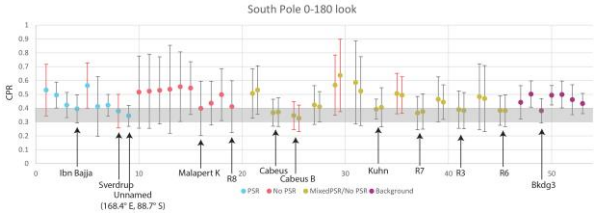

Figure 2: Mini-RF east-looking CPR data for all analyzed craters and background regions. Red error bars denote craters also analyzed by [9], and "R" denotes craters derived from the analysis database of [8]. The gray region highlights a region of exceptionally low CPR.

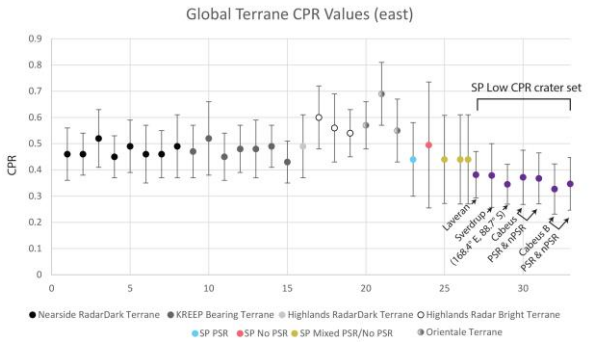

Figure 3: Comparison of global terrain CPR trends [11] with the 5 exceptionally low CPR south polar craters. The magnitude of CPR difference suggests that these craters should be classified as a distinct terrain type, possibly linked to the volatile properties of the near-surface regolith.

References: [1] Feldman, W. C., et al. (1998) *Science, 281*, 1496-1500. [2] Lawrence, D. J., et al. (2006) *JGR Planets, 111*, E8. [3] Colaprete, A., et al. (2010) *Science 330*, 463-468. [4] Hayne, P. O., et al. (2015) *Icarus, 255*, 58-69. [5] Li, S., et al. (2018) *PNAS, 115*, 8907-8912. [6] Hapke, B. W., et al. (1993) *Science, 260*, 509-511. [7] Neish, C. D., et al. (2011) *JGR Planets, 116*, E1. [8] Rubanenko, L., et al. (2019) *Nature Geoscience, 12*, 597-601. [9] Deutsch, A. N., (2021) *LPSC 52*, Abstract #2019. [10] Kirk, R. L., et al. (2013) *LPSC 44*, Abstract #2920. [11] Cahill, J. T. S., et al. (2014) *Icarus, 243*, 173-190.